

RESEARCH ARTICLE | SEPTEMBER 20 2022

Optimizing speckles for dynamic objects using genetic algorithm in ghost imaging

Yuchen He  ; Shuai Mao; Juan Chen; Yuan Yuan   ; Hui Chen  ; Zhuo Xu



AIP Advances 12, 095012 (2022)

<https://doi.org/10.1063/5.0096821>

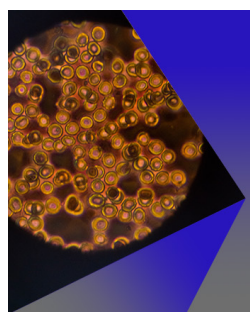


View
Online



Export
Citation

CrossMark



AIP Advances

Special Topic: Medical Applications
of Nanoscience and Nanotechnology

Submit Today!

 AIP
Publishing

Optimizing speckles for dynamic objects using genetic algorithm in ghost imaging

Cite as: AIP Advances 12, 095012 (2022); doi: 10.1063/5.0096821

Submitted: 22 April 2022 • Accepted: 28 July 2022 •

Published Online: 20 September 2022



View Online



Export Citation



CrossMark

Yuchen He,¹ Shuai Mao,² Juan Chen,² Yuan Yuan,^{1,a} Hui Chen,¹ and Zhuo Xu¹

AFFILIATIONS

¹ Electronic Materials Research Laboratory, Key Laboratory of the Ministry of Education and International Center for Dielectric Research, School of Electronic Science and Engineering, Xi'an Jiaotong University, Xi'an 710049, China

² School of Information and Communications Engineering, Xi'an Jiaotong University, Xi'an 710049, China

^aAuthor to whom correspondence should be addressed: yuanyuan0@xjtu.edu.cn

ABSTRACT

Different from the traditional imaging methods using first-order interference, ghost imaging (GI) uses the second-order correlation, bringing many potential applications. On the other hand, GI has been suffering from low efficiency in image reconstruction due to a high sampling rate, which is a barrier for its application, especially when dealing with dynamic objects. The genetic algorithm (GA) can optimize the speckle sequence for an object and enable GI reconstruction with a few speckle patterns. However, the optimized speckle sequence of the GA usually loses the generalization and can only reconstruct the object being tested, making it far from suitable for handling a dynamic object. Here, we propose an improved method based on the GA, where we make two selection rules: the selective patterns more likely have a high response from the object, and meanwhile, the selected patterns tend to be linearly independent from each other. The optimized speckle sequence under these rules not only results in successful reconstruction but also preserves a generalization to a certain extent, enabling the GI to reconstruct the different states of the dynamic object at a low overall sampling rate. In the verification of the first frame, our method performs better based on the demonstration of various algorithms. In a demonstration of the dynamic object at 50% sampling rate, the reconstructed images are 2.1775 dB higher at 12 different frames on average in the peak signal-to-noise ratio than the random speckle sequence.

© 2022 Author(s). All article content, except where otherwise noted, is licensed under a Creative Commons Attribution (CC BY) license (<http://creativecommons.org/licenses/by/4.0/>). <https://doi.org/10.1063/5.0096821>

17 August 2023 13:23:57

I. INTRODUCTION

Since Pittman *et al.* demonstrated the first ghost imaging (GI) experiment in 1995, it has been developed as a novel imaging method for more than 20 years.¹ GI uses second-order correlation to achieve image reconstruction, which brings features such as being lens-less and turbulence-free and having a high resolution. GI has attracted the attention of many researchers and achieved attractive results,^{2–17} but it also suffers from the trade-off between image quality and the sampling rate (the number of patterns divided by the total number of resolution pixels). High image quality requires a pretty high sampling rate that slows down the imaging speed, hindering the application of GI for dynamic objects. Compressed sensing (CS) algorithms have been introduced into GI to solve this problem, but its effect is limited by the high computational cost.^{12,18–21} Artificial intelligence (AI) methods are also considered a possible way to improve this situation, but generally there are limitations,^{22–29}

such as being strongly dependent on the feature and volume of the training set. The methods mentioned above use general speckle patterns rather than considering the special structure of an object.

The genetic algorithm (GA), a kind of randomized search algorithm based on the natural selection and natural genetic mechanism of biology,³⁰ was recently introduced to GI. In 2017, a background subtraction method using the GA for a GI system was proposed, which can eliminate the background noise.³¹ However, this method is not suitable for traditional computational ghost imaging (CGI). A GA-based optimization method for the space structure of speckles in GI was proposed in 2018, which utilizes fewer sub-sources to overcome periodicity of the light field and obtain a better result.³² Essentially, that work's objective was to optimize the structure and property of the pseudo-thermal light field. In 2021, an adaptive speckle optimization imaging method SEGI was proposed, which utilized the GA to make the speckle gradually closer to the target

image.³³ SEGI abandons the traditional image reconstruction process and improves the imaging effect mainly in two ways. One is by increasing the optimization generation, which will increase the imaging time and complexity of the system. The other depends on the degree of exploration of cross inheritance and variation, and the difficulty of fast convergence to the optimal solution will limit the improvement in imaging quality. Simultaneously, the optimized speckle patterns are highly associated with the object and will work worse for another object with a different look. This feature makes it far from dealing with a dynamic object whose image changes with time.

Here, we propose an improved method based on the GA, aiming to image a dynamic object with an overall small number of speckle patterns. Mathematically, GI performs an expansion of an object on a set of bases. The bases are the speckle patterns, and the bucket signals are the corresponding weights. A very high weight means the corresponding pattern looks very close to the object. A very low weight means the pattern has a quite opposite (rather than different) look to the object. Therefore, the patterns of the largest and lowest weights (called responsive terms) help in faster image reconstruction than the ones close to the means of the bucket signal (called unresponsive terms). However, if we only select very few responsive terms, GI will lose the generalization ability. Even a small change in the object would result in an unacceptable reconstructed image. To avoid this phenomenon, we setup two selection rules: the responsive terms are more likely to be chosen, and the selected patterns are linear independent to each other. When handling a dynamic object, we use the first frame for initial optimization, and then the remaining frame is illuminated by the optimized speckle sequence from the previous frame.

We first demonstrated the first frame of the target ("XJTU") using eight different algorithms, and the results show that the peak signal to noise ratio (PSNR) of the proposed method is 1.84 and

3.43 dB higher (at 25% and 50% sampling rates, respectively) on average than those based on the original speckle patterns. Furthermore, we performed a demonstration on a complex object (real scene in our hometown) and compared it with the total variation algorithm (TV). The proposed method improves the PSNR by 4.2691 and 3.766 dB at 25% and 50% sampling rates, respectively. Finally, we rotated and translated the object "XJTU" to 12 different positions. The results show that the proposed method is 2.1775 dB higher at 12 different frames on average in the PSNR than the random speckle sequence. Figure 1 shows the schematic diagram of the proposed method.

II. THE PROPOSED METHOD

A. Principle

In a CGI system, a preset speckle sequence is employed to illuminate the target, and the corresponding echo signal is collected through the bucket detector without spatial resolution. The detection process can be expressed as follows:

$$S_{bi} = \int S_i(\xi) \cdot O(\xi) d\xi, \quad (1)$$

where S_{bi} is the bucket signal corresponding to the i -th detection, $S_i(\xi)$ is the speckle used for the i -th illumination, and $O(\xi)$ is the transmission or reflection function of the target. The traditional GI algorithm utilizes coincidence calculation for image reconstruction. The process can be expressed as

$$O(\xi) = \frac{1}{M} \sum_{i=1}^M (S_{bi} - \langle S_{bi} \rangle) \cdot S_i(\xi), \quad (2)$$

where $\langle \cdot \rangle$ represents the system average and M represents the number of illuminations. Although this algorithm is simple and direct, it

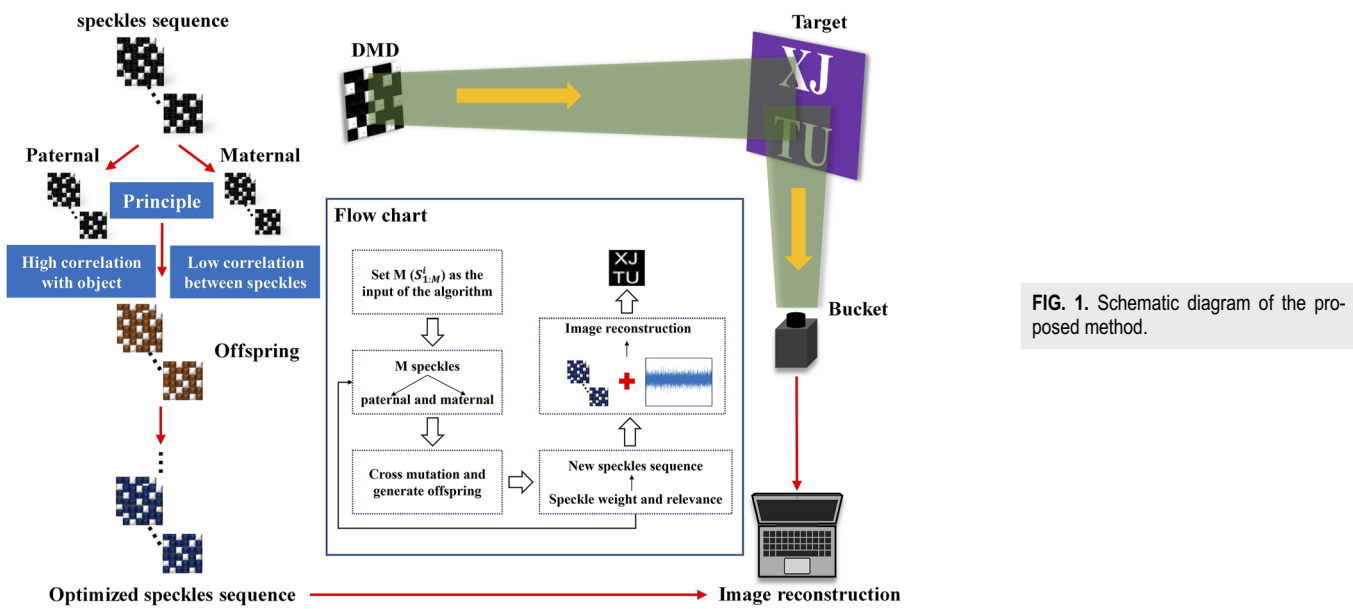


FIG. 1. Schematic diagram of the proposed method.

will also bring background noise in the accumulation process. It can be seen from Eq. (2) that the result of image reconstruction is the accumulation of speckles with different weights and that the weight coefficient ω is the difference between the i -th bucket signal and the mean value of the bucket signals ($S_{bi} - \langle S_{bi} \rangle$). When $\omega > 0$, the larger the ω , the more target information it contains. On the other hand, when $\omega < 0$, the smaller the ω , the more information about other parts in the imaging area it contains (which can effectively reduce the pixel value of the area without a target). From the analysis mentioned above, we can draw a conclusion that the larger the value of $|\omega|$, the more conducive the corresponding speckle will be to image reconstruction. Simultaneously, in view of the mechanism of GI, it is necessary to ensure the time-space independent feature of the speckle sequence. Consequently, we consider the weight and speckle as two factors combined with the GA to optimize the performance of GI. The larger the weight, the higher the correlation with the object. The lower the correlation between speckles, the better the time-space independence feature.

B. Method

The proposed method in this paper mainly includes five parts: speckle input, inheritance, variation, evolution, and imaging.

- (1) Speckle input: set the random speckles to $S_{1:M}^i$, and the pixel value at each position of the speckle $S(\xi)$ is used as the genetic information.
- (2) Inheritance: in the i -th generation of the GA, the input random speckle set $S_{1:M}^i$ will be randomly divided into two parts: paternal speckle set S_{fes}^i and maternal speckle set S_{mos}^i . Then, cross inheritance was performed P (hyper-parameter) times and the offspring speckle set S_{chs}^i was generated. The larger the value of P , the higher the degree of exploration, and the better the optimization result. In the process of cross inheritance, P paternal speckles and P maternal speckles are randomly selected from the corresponding set. The genetic information is randomly crossed to generate the offspring speckle set S_{chs}^i . The offspring speckle is the combination of the speckle randomly selected from the paternal set and the speckle randomly selected from the maternal set. The proportion of speckles in paternal or maternal sets can be controlled by the hyper-parameter exchange probability $p_{crossover}^{size}$.
- (3) Variation: to increase the degree of exploration and prevent premature convergence of the optimization process, the offspring speckle set S_{chs}^i will undergo a variation process. Each offspring speckle S_{child}^i has a certain probability of variation. The genetic information at some positions will change randomly, and the size of the variation position can be controlled by the hyper-parameter p_{mutate}^{size} .
- (4) Evolution: after (2) and (3), there are M parental speckles $S_{1:M}^i$ and P offspring speckles S_{chs}^i . In the process of evolution, the next generation of M parental speckles $S_{1:M}^{i+1}$ will be selected from $(M+P)$ speckles. Then, the selection of speckle patterns is according to $|\omega|$. The larger the value of $|\omega|$, the more likely the corresponding speckle will be selected. With the optimization process of the GA, it will gradually converge to the local optimal solution, and the similarity between speckles will gradually increase. Therefore, the newly selected

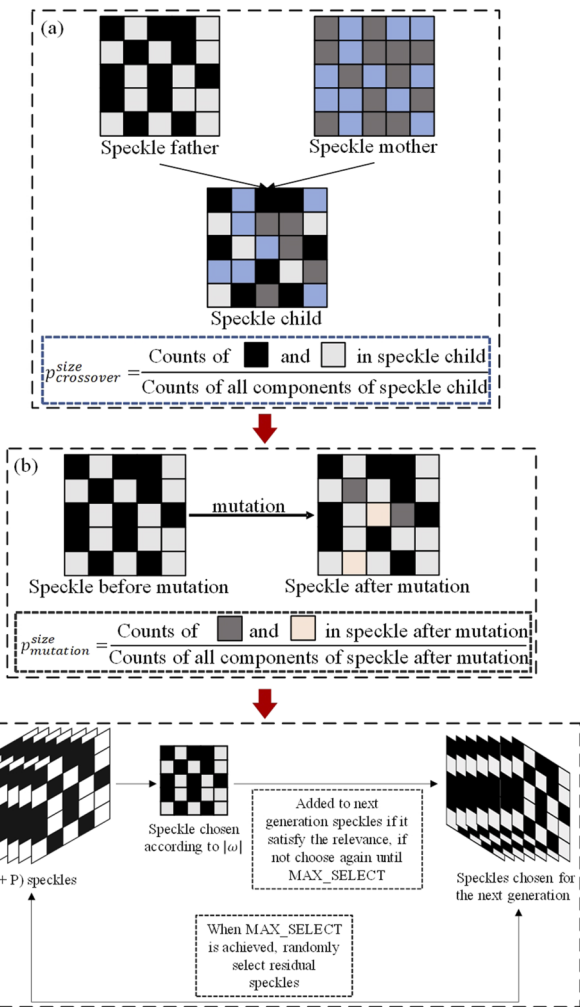


FIG. 2. Schematic diagram of speckle optimization: (a) inheritance, (b) variation, and (c) evolution.

speckle will be compared with the previously selected speckle in the process of natural selection. To avoid the optimization process falling into a long cycle, the maximum number of selections will be set as a hyper-parameter MAX_SELECT. When the maximum is reached, the remaining speckle will be randomly selected.

- (5) Imaging: finally, the optimized speckle and the corresponding bucket signal are utilized for image reconstruction.

Figure 2 shows the schematic diagram of inheritance, variation, and evolution.

III. DEMONSTRATION RESULTS

A. Settings

In this work, the number of cross inheritances $P = M$, that is, the number of speckles in the offspring is the same as that in

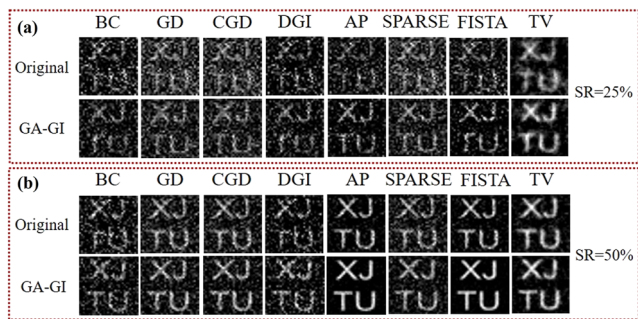


FIG. 3. Comparison results on the first frame. (a) Results at 25% sampling rate. (b) Results at 50% sampling rate.

the parental one. $p_{crossover}^{size} = 0.5$, that is, the average number of the selected exchange position is stable at half of the total size of the target. $p_{crossover}^{size} = 0.3$, that is, each speckle has a 30% probability of mutation. $p_{mutate}^{size} = 0.1$, that is, the mean value of the mutated position is stable at one tenth of the total size of the target. The letters "XJTU" are regarded as the target with a resolution of 32×32 . Based on the framework of CGI, we utilize eight different algorithms to demonstrate the proposed algorithm, namely, BC, gradient descent (GD), conjugate gradient descent (CGD), differential ghost imaging (DGI), alternating projection (AP), SPARSE, the fast iterative shrinkage-thresholding algorithm (FISTA), and total variation (TV).^{34–40}

B. Results on the first frame

First, we validate the proposed method on the first frame at 25% and 50% sampling rates based on the real speckle sequence generated

by (digital micromirror devices) DMD. Each algorithm is compared with the original state and the proposed method. The results are shown in Fig. 3.

The proposed method (GA-GI) can produce better results on the first frame, and Table I lists the specific values. The PSNR of the proposed method is 1.84 and 3.43 dB higher (25% and 50% sampling rates, respectively) on average than those based on the original speckle sequence. Notably, GA-GI improves the PSNR of FISTA by 2.4957 and 9.6825 dB, respectively.

Furthermore, we demonstrate the first frame optimization on a complex object (real scene in our hometown) (64×64) and choose the TV algorithm at 25% and 50% sampling rates for comparison. Figure 4 shows that through the optimization of the proposed method, the result at 25% sampling rate improves to 4.2691 dB, and the result at 50% sampling rate improves to 3.766 dB.

C. Results on the dynamic object

Finally, we demonstrate the proposed method on a dynamic object. We make the target "XJTU" rotation ($5^\circ, 10^\circ, 15^\circ, 20^\circ, 25^\circ$, and 30°) and downward movement (1 pixel, 2 pixels, 3 pixels, 4 pixels, 5 pixels, and 6 pixels). The speckle sequence used for illumination in each subsequent frame is optimized based on the previous frame. For example, the speckle sequence in the 5° or 1 pixel scene is optimized from the first frame (static frame). Each state of motion is compared with the speckle sequence randomly generated at 50% sampling rates (by FISTA). Figure 5 shows the comparison results.

In Figs. 5(a) and 5(b), we show the dynamic object (XJTU), the results of the random speckle sequence (original), and the results of the proposed method (GA-GI). Obviously, GA-GI can provide a better visual result, and Table II lists the specific values.

TABLE I. Numerical results on the first frame (Boldface denotes the specific increment value).

25% sampling rate [PSNR (dB)/SSIM]				
	BC	GD	CGD	DGI
Original	11.1791/0.2414	11.0765/0.2484	11.1381/0.2494	11.6251/0.2512
GA-GI	12.4893/0.2872	12.5791/0.3058	12.6432/0.309	12.6723/0.3022
Increment	1.3102/0.0458	1.5026/0.0574	1.5051/0.0596	1.0472/0.051
	AP	SPARSE	FISTA	TV
Original	11.8493/0.2394	11.041/0.2553	11.944/0.2726	14.6949/0.4504
GA-GI	14.2671/0.4341	13.4036/0.3521	14.4397/0.447	16.7808/0.5602
Increment	2.4178/0.1947	2.3626/0.0968	2.4957/0.1744	2.0859/0.1098
50% sampling rate [PSNR (dB)/SSIM]				
	BC	GD	CGD	DGI
Original	12.5701/0.3276	14.0598/0.4098	14.3273/0.421	13.067/0.3484
GA-GI	13.8092/0.3924	15.5221/0.4773	16.1055/0.5048	14.1251/0.4259
Increment	1.2391/0.0648	1.4623/0.0675	1.7782/0.0838	1.0581/0.0775
	AP	SPARSE	FISTA	TV
Original	18.5395/0.6384	14.2384/0.4158	18.7216/0.6395	18.4809/0.6161
GA-GI	26.5077/0.8833	16.5604/0.5205	28.4041/0.9029	20.4161/0.6814
Increment	7.9682/0.2449	2.322/0.1047	9.6825/0.2634	1.9352/0.0653

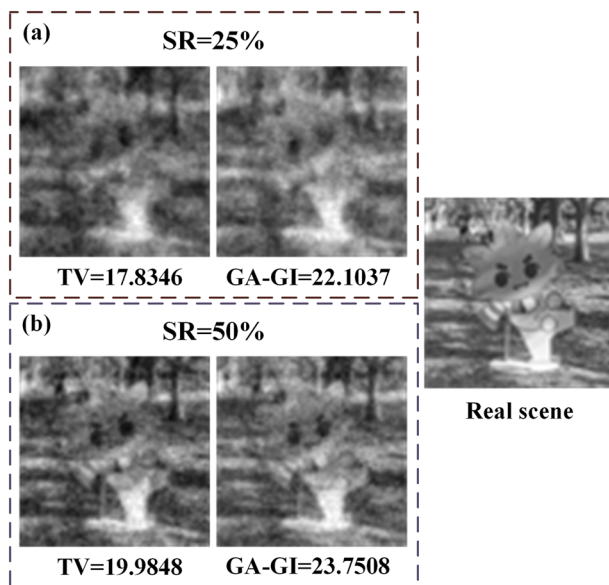


FIG. 4. Results on the real scene. (a) Results at 25% sampling rate. (b) Results at 50% sampling rate.

GA-GI is 2.1386 dB/0.0845 higher and 2.2163 dB/0.1019 higher on average (PSNR/SSIM) than the results based on the random speckle sequence at six different positions and six different rotations.

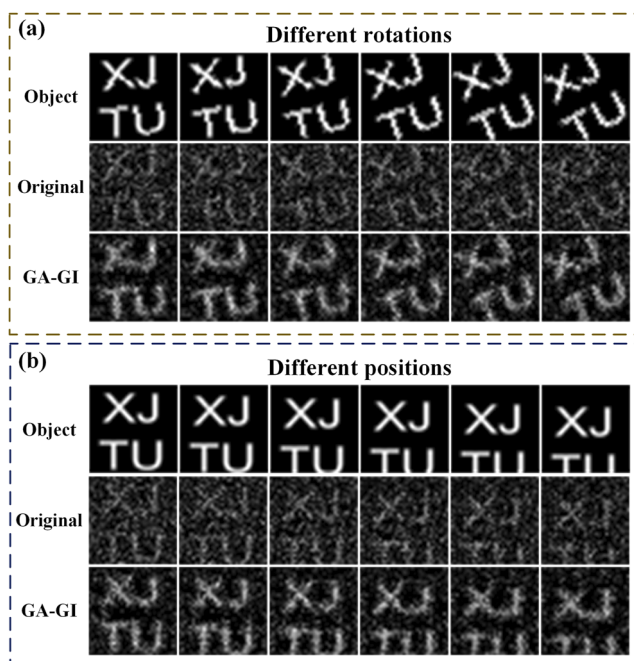


FIG. 5. Results on the dynamic object. (a) Results at different rotations. (b) Results at different positions.

TABLE II. Numerical results on the dynamic object.

Pixel	PSNR (dB)					
	1	2	3	4	5	6
Random	14.9325	15.0227	15.3580	15.6257	15.7986	15.5803
GA-GI	17.1166	17.5558	16.4073	17.8741	17.4627	18.7329
Increment	2.1841	2.5331	1.0493	2.2484	1.6641	3.1526
Rotation	5 Å	10 Å	15 Å	20 Å	25 Å	30 Å
Random	15.2997	14.9166	15.0778	14.7228	14.6802	14.6708
GA-GI	17.6991	16.0751	17.2812	17.1652	17.4601	16.9852
Increment	2.3994	1.1585	2.2034	2.4424	2.7799	2.3144

Pixel	SSIM					
	1	2	3	4	5	6
Random	0.4440	0.4401	0.4432	0.4301	0.4191	0.3872
GA-GI	0.5525	0.5484	0.4859	0.5100	0.4793	0.4944
Increment	0.1085	0.1083	0.0427	0.0799	0.0602	0.1072
Rotation	5 Å	10 Å	15 Å	20 Å	25 Å	30 Å
Random	0.4775	0.4625	0.4593	0.4374	0.4227	0.4288
GA-GI	0.5755	0.5249	0.5490	0.5591	0.5557	0.5351
Increment	0.0980	0.0624	0.0897	0.1217	0.133	0.1063

IV. CONCLUSION

In this paper, we present a GA-based GI method, aiming to image a dynamic object with an overall small number of illumination patterns. We select high correlation with the object and low correlation between speckles as two principles of the optimization method. Then, we use the speckle sequence obtained by optimizing the previous frame of the object to illuminate the scene in the following frames. We carried out a series of demonstrations based on real speckle sequences projected by DMD to verify the proposed method and compared it with various algorithms under different sampling rates. Extensive results show that the proposed optimization method achieves promising performance for each frame in the scene and that it can obtain optimal results both in the PSNR and SSIM.

ACKNOWLEDGMENTS

This work was supported, in part, by the National Natural Science Foundation of China (Grant No. 61901353), the Fundamental Research Funds for the Central Universities (Grant No. xhj032021005), the Key Research and Development Projects of Shaanxi Province (Grant No. 2021GXZH-Z-012), and the 111 Project of China (Grant No. B14040).

AUTHOR DECLARATIONS

Conflict of Interest

The authors have no conflicts to disclose.

Author Contributions

Yuchen He: Conceptualization (lead); Writing – review & editing (lead). **Shuai Mao:** Data curation (equal). **Juan Chen:** Investigation

(equal). **Yuan Yuan:** Methodology (equal). **Hui Chen:** Data curation (equal). **Zhuo Xu:** Supervision (equal).

DATA AVAILABILITY

The data that support the findings of this study are available from the corresponding author upon reasonable request.

REFERENCES

- ¹T. B. Pittman, Y. H. Shih, D. V. Strekalov, and A. V. Sergienko, "Optical imaging by means of two-photon quantum entanglement," *Phys. Rev. A* **52**, R3429 (1995).
- ²A. F. Abouraddy, B. E. A. Saleh, A. V. Sergienko, and M. C. Teich, "Role of entanglement in two-photon imaging," *Phys. Rev. Lett.* **87**, 123602 (2001).
- ³R. S. Bennink, S. J. Bentley, and R. W. Boyd, "Two-photon coincidence imaging with a classical source," *Phys. Rev. Lett.* **89**, 113601 (2002).
- ⁴A. Gatti, E. Brambilla, M. Bache, and L. A. Lugiato, "Ghost imaging with thermal light: Comparing entanglement and classical correlation," *Phys. Rev. Lett.* **93**, 093602 (2004).
- ⁵R. S. Bennink, S. J. Bentley, R. W. Boyd, and J. C. Howell, "Quantum and classical coincidence imaging," *Phys. Rev. Lett.* **92**, 033601 (2004).
- ⁶A. Valencia, G. Scarcelli, M. D'Angelo, and Y. Shih, "Two-photon imaging with thermal light," *Phys. Rev. Lett.* **94**, 063601 (2005).
- ⁷F. Ferri, D. Magatti, A. Gatti, M. Bache, E. Brambilla, and L. A. Lugiato, "High-resolution ghost image and ghost diffraction experiments with thermal light," *Phys. Rev. Lett.* **94**, 183602 (2005).
- ⁸L. Basano and P. Ottomello, "Experiment in lensless ghost imaging with thermal light," *Appl. Phys. Lett.* **89**, 091109 (2006).
- ⁹G. Scarcelli, V. Berardi, and Y. Shih, "Can two-photon correlation of chaotic light be considered as correlation of intensity fluctuations?," *Phys. Rev. Lett.* **96**, 063602 (2006).
- ¹⁰J. H. Shapiro, "Computational ghost imaging," *Phys. Rev. A* **78**, 061802(R) (2008).
- ¹¹R. Meyers, K. S. Deacon, and Y. Shih, "Ghost-imaging experiment by measuring reflected photons," *Phys. Rev. A* **77**, 041801(R) (2008).
- ¹²O. Katz, Y. Bromberg, and Y. Silberberg, "Compressive ghost imaging," *Appl. Phys. Lett.* **95**, 131110 (2009).
- ¹³R. E. Meyers, K. S. Deacon, and Y. Shih, "Turbulence-free ghost imaging," *Appl. Phys. Lett.* **98**, 111115 (2011).
- ¹⁴M. F. Li, Y. R. Zhang, X. F. Liu, X. R. Yao, K.-H. Luo, H. Fan, and L.-A. Wu, "A double-threshold technique for fast time-correspondence imaging," *Appl. Phys. Lett.* **103**, 211119 (2013).
- ¹⁵D. J. Zhang, Q. Tang, T. F. Wu, H. C. Qiu, D. Q. Xu, H. G. Li, H. B. Wang, J. Xiong, and K. Wang, "Lensless ghost imaging of a phase object with pseudo-thermal light," *Appl. Phys. Lett.* **104**, 121113 (2014).
- ¹⁶D. Pelliccia, A. Rack, M. Scheel, V. Cantelli, and D. M. Paganin, "Experimental x-ray ghost imaging," *Phys. Rev. Lett.* **117**, 113902 (2016).
- ¹⁷R. I. Khakimov, B. M. Henson, D. K. Shin, S. S. Hodgman, R. G. Dall, K. G. H. Baldwin, and A. G. Truscott, "Ghost imaging with atoms," *Nature* **540**, 100–103 (2016).
- ¹⁸V. Katkovnik and J. Astola, "Compressive sensing computational ghost imaging," *J. Opt. Soc. Am. A* **29**, 1556–1567 (2012).
- ¹⁹M. Amann and M. Bayer, "Compressive adaptive computational ghost imaging," *Sci. Rep.* **3**, 1545 (2013).
- ²⁰L. Long-Zhen, Y. Xu-Ri, L. Xue-Feng, Y. Wen-Kai, and Z. Guang-Jie, "Super-resolution ghost imaging via compressed sensing," *Acta Phys. Sin.* **63**, 224201 (2014).
- ²¹H. Zhang, Y. Xia, and D. Duan, "Computational ghost imaging with deep compressed sensing," *Chin. Phys. B* **30**, 124209 (2021).
- ²²M. Lyu, W. Wang, H. Wang, H. Wang, G. Li, N. Chen, and G. Situ, "Deep-learning-based ghost imaging," *Sci. Rep.* **7**, 17865 (2017).
- ²³T. Shimobaba, Y. Endo, T. Nishitsui, T. Takahashi, Y. Nagahama, S. Hasegawa, M. Sano, R. Hirayama, T. Kakue, A. Shiraki, and T. Ito, "Computational ghost imaging using deep learning," *Opt. Commun.* **413**, 147–151 (2018).
- ²⁴Y. He, G. Wang, G. Dong, S. Zhu, H. Chen, A. Zhang, and Z. Xu, "Ghost imaging based on deep learning," *Sci. Rep.* **8**, 6469 (2018).
- ²⁵S. Ota, R. Horisaki, Y. Kawamura, M. Ugawa, I. Sato, K. Hashimoto, R. Kamesawa, K. Setoyama, S. Yamaguchi, K. Fujii, K. Waki, and H. Noji, "Ghost cytometry," *Science* **360**, 1246–1251 (2018).
- ²⁶T. Bian, Y. Yi, J. Hu, Y. Zhang, Y. Wang, and L. Gao, "A residual-based deep learning approach for ghost imaging," *Sci. Rep.* **10**, 12149 (2020).
- ²⁷H. Wu, R. Wang, G. Zhao, H. Xiao, D. Wang, J. Liang, X. Tian, L. Cheng, and X. Zhang, "Sub-Nyquist computational ghost imaging with deep learning," *Opt. Express* **28**, 3846–3853 (2020).
- ²⁸Z. Zhang, C. Wang, W. Gong, and D. Zhang, "Ghost imaging of blurred object based on deep-learning," *Appl. Opt.* **60**, 3732–3739 (2021).
- ²⁹Y. He, S. Duan, Y. Yuan, H. Chen, J. Li, and Z. Xu, "Semantic ghost imaging based on recurrent-neural-network," *Opt. Express* **30**, 23475–23484 (2022).
- ³⁰J. H. Holland, *Adaptation in Natural and Artificial Systems: An Introductory Analysis with Applications to Biology, Control, and Artificial Intelligence* (MIT press, 1975).
- ³¹M. Zafari, S. Ahmadi-Kandjani, and R. Kheradmand, "Noise reduction in selective computational ghost imaging using genetic algorithm," *Opt. Commun.* **387**, 182–187 (2017).
- ³²H. Wu, C. Wang, and W. Gong, "Ghost imaging via sparse structured illumination source," *Opt. Express* **26**, 4183 (2018).
- ³³B. Liu, F. Wang, C. Chen, F. Dong, and D. McGloin, "Self-evolving ghost imaging," *Optica* **8**, 1340–1349 (2021).
- ³⁴S.-i. Amari, "Backpropagation and stochastic gradient descent method," *Neurocomputing* **5**, 185–196 (1993).
- ³⁵G. Yuan, X. Lu, and Z. Wei, "A conjugate gradient method with descent direction for unconstrained optimization," *J. Comput. Appl. Math.* **233**, 519–530 (2009).
- ³⁶F. Ferri, D. Magatti, L. A. Lugiato, and A. Gatti, "Differential ghost imaging," *Phys. Rev. Lett.* **104**, 253603 (2010).
- ³⁷H. Liu and J. Peng, "Sparse signal recovery via alternating projection method," *Signal Process.* **143**, 161 (2018).
- ³⁸Z. Lin, M. Chen, and Y. Ma, "The augmented Lagrange multiplier method for exact recovery of corrupted low-rank matrices," *arXiv:1009.5055* (2010).
- ³⁹A. Beck and M. Teboulle, "A fast iterative shrinkage-thresholding algorithm for linear inverse problems," *SIAM J Imaging Sci.* **2**, 183–202 (2009).
- ⁴⁰O. E. Fatemi, "Nonlinear total variation based noise removal algorithms," *Physica D* **60**, 259 (1992).